PAPER

Conservation of quantum efficiency in quantum well intermixing by stress engineering with dielectric bilayers

To cite this article: Seval Arslan *et al* 2018 *Semicond. Sci. Technol.* **33** 025001

View the article online for updates and enhancements.

Related content

- Impurity-free quantum well intermixing for large optical cavity high-power laser diode structures
Abdullah Kahraman, Emre Gür and Atilla Aydnl

- Investigations of impurity-free vacancy disordering in (Al)InGaAs(P)/InGaAs quantum wells
S C Du, L Fu, H H Tan et al.

- Fabrication of wavelength-shifted In0.2Ga0.8As/GaAs MQW laser diodes by IFVD at different thermal annealing temperatures
Jae Su Yu, Jin Dong Song, Yong Tak Lee et al.

IOP ebooks™

Bringing you innovative digital publishing with leading voices to create your essential collection of books in STEM research.

Start exploring the collection - download the first chapter of every title for free.

Conservation of quantum efficiency in quantum well intermixing by stress engineering with dielectric bilayers

Seval Arslan[1], Abdullah Demir[1] , Seval Şahin[2] and Atilla Aydınlı[3]

[1] Department of Physics, Bilkent University, 06800, Ankara, Turkey
[2] Department of Physics, Anadolu University, 26470, Eskişehir, Turkey
[3] Department of Electrical and Electronics Engineering, Uludağ University, 16059, Bursa, Turkey

E-mail: abdullah.demir@bilkent.edu.tr and atillaaydinli@uludag.edu.tr

CrossMark

Abstract

In semiconductor lasers, quantum well intermixing (QWI) with high selectivity using dielectrics often results in lower quantum efficiency. In this paper, we report on an investigation regarding the effect of thermally induced dielectric stress on the quantum efficiency of quantum well structures in impurity-free vacancy disordering (IFVD) process using photoluminescence and device characterization in conjunction with microscopy. SiO_2 and Si_xO_2/SrF_2 (versus SrF_2) films were employed for the enhancement and suppression of QWI, respectively. Large intermixing selectivity of 75 nm (125 meV), consistent with the theoretical modeling results, with negligible effect on the suppression region characteristics, was obtained. Si_xO_2 layer compensates for the large thermal expansion coefficient mismatch of SrF_2 with the semiconductor and mitigates the detrimental effects of SrF_2 without sacrificing its QWI benefits. The bilayer dielectric approach dramatically improved the dielectric–semiconductor interface quality. Fabricated high power semiconductor lasers demonstrated high quantum efficiency in the lasing region using the bilayer dielectric film during the intermixing process. Our results reveal that stress engineering in IFVD is essential and the thermal stress can be controlled by engineering the dielectric strain opening new perspectives for QWI of photonic devices.

(Some figures may appear in colour only in the online journal)

1. Introduction

Even though record high output powers have been demonstrated for semiconductor lasers [1–4], one of the limitations for high laser output power operation is the catastrophic optical mirror damage (COMD) [5]. Among various facet engineering techniques to suppress COMD, quantum well intermixing (QWI) is preferred because it is easier to implement and laser design and COMD suppression windows can be realized independently [6–9]. QWI has been exploited for the monolithic integration of tunable semiconductor lasers, low-loss waveguides, modulators and photodetectors [10–12].

Effective bandgap of the QW is enlarged by interdiffusion of the atoms across it in the QWI window so that losses due to interband absorption in the output window region are substantially reduced or even eliminated. One of the most promising QWI approaches is impurity-free vacancy disordering (IFVD) since it does not introduce additional impurities and hence eliminates free carrier absorption losses and, in the ideal case, preserves epitaxial quality [6]. The IFVD process requires the deposition of a dielectric cap to control the degree of intermixing to be enhanced or suppressed with the appropriate dielectric materials and annealing temperature [7, 9, 13–17]. The vacancy disordering is mainly affected by

the dielectric film and the thermal stress executed by the dielectric film on the semiconductor [18].

Studies on IFVD have focused more on wavelength control or fabrication of multiwavelength lasers [7, 15, 16]. Work with an emphasis on achieving large intermixing selectivity with minimal wavelength and quantum efficiency disruption in the suppression region has so far been scarce with limited disclosure of the applied technique [19–21]. Device lifetime and operational powers of high power laser diodes with a non-absorbing output window were reported to be highly correlated with the amount of QWI selectivity, i.e. the PL wavelength (bandgap) shift difference $\Delta\lambda$ (ΔE) between the gain and IFVD window regions [19, 20]. Naito et al demonstrated that semiconductor lasers with larger ΔE operate at higher output power with longer device lifetime and stable operation of more than 5000 h at 20 W output was achieved for 9xx nm broad area laser diodes using IFVD windows with $\Delta E = 100$ meV [20]. Intermixing by SiO_2 and suppression by Si_xO_2 ($x > 1$) or Si_3N_4 caps offers high quantum efficiency and surface quality but lacks good QWI selectivity [13, 16]. Intermixing by SiO_2 and suppression under SrF_2 caps were demonstrated with good QWI selectivity; however, SrF_2-capped laser devices suffered from a penalty on operational voltage, threshold current, quantum efficiency [22–24] and some surface damage was apparent after annealing [7], which needs to be avoided for reliable operation of these devices. The surface defects indicate degradation of the epitaxial material quality and under high injection current densities defects can migrate into the active region and promote the non-radiative recombination, which increases threshold current and decreases the quantum efficiency and reliable output power of the high power laser diodes. Understanding and solving these issues are keys to attain high-performance optoelectronic devices with reliable long operation lifetimes.

In this study, we investigated the effect of thermal stress on the quantum efficiency of the devices using SiO_2 for QWI and SrF_2 single-layer versus Si_xO_2/SrF_2 bilayer for QWI suppression with large selectivity. Si_xO_2 layer compensates for the large thermal expansion coefficient mismatch of SrF_2 with the semiconductor and hence the bilayer approach mitigates the detrimental effects of SrF_2 without sacrificing its QWI selectivity benefits. By comparing SrF_2 and strain-compensated Si_xO_2/SrF_2 films, the effect of thermally induced dielectric stress on the epitaxial structure and laser performance were demonstrated. High intermixing selectivity of 75 nm (125 meV) with negligible effect in the suppression region was obtained using Si_xO_2/SrF_2. Utilizing the bilayer dielectric for intermixing suppression, we demonstrate an IFVD process for high power semiconductor lasers with good surface morphology, large QWI selectivity, high quantum efficiency and negligible effect on lasing characteristics. Our results reveal that the thermal stress due to QWI process can be controlled by engineering the dielectric strain and open new perspectives for QWI of photonic devices.

2. Experimental details

Laser structure was grown by metalorganic chemical vapor deposition on GaAs. The structure was composed of 3000 nm n-AlGaAs cladding, 500 nm n-AlGaAs waveguide, 8 nm InGaAs QW, 500 nm p-AlGaAs waveguide, 1000 nm p-AlGaAs cladding, and finally capped by 100 nm GaAs contact layer. Plasma enhanced chemical vapor deposition (PECVD) was used for SiO_2 and Si_xO_2 depositions, and thermal evaporation was implemented for SrF_2 deposition process. The refractive indices of the deposited films were measured by spectroscopic ellipsometry as 1.46 for SiO_2, 1.57 for Si_xO_2 and 1.38 for SrF_2 at 633 nm.

Single layer and bilayer films were studied in this work. For the investigation of single layer film effect, 250 nm thick SiO_2, Si_xO_2 and SrF_2 dielectric films were used. For comparison of the QWI suppression, 10 nm/30 nm thick Si_xO_2/SrF_2 bilayer films and 30 nm thick SrF_2 film were used. The deposition recipe for Si_xO_2 was developed to yield smaller wavelength shifts compared to SiO_2 by changing its stoichiometry through modification of flow rates in PECVD [16]. For the multilayer films, two distinct regions were defined, where the first one is for QWI (SiO_2) and the second is for QWI suppression (SrF_2 versus Si_xO_2/SrF_2). Initially, 250 nm SiO_2 intermixing dielectric was deposited on (5 mm) $\times$ (10 mm) wafer samples and a half of it was etched. Then, either 1-layer (30 nm-SrF_2) or 2-layer (10 nm-Si_xO_2/30 nm-SrF_2) dielectrics were deposited on the whole sample. The side view of the dielectric deposition configuration is shown in figure 1(a1) and (a2). Rapid thermal annealing (RTA) from 860 to 920 °C for 2 min were carried out in nitrogen ambient by sandwiching the samples between fresh GaAs wafers to prevent out-diffusion of As atoms from the surface of the samples. Extended time annealing (2–6 min) at 880 °C were also performed to increase the QWI selectivity. After removal of the dielectrics, surface quality was evaluated by optical and atomic force microscopy (AFM). To estimate the amount of QWI, room temperature PL measurements were performed from the top after etching off ∼1 μm of the epitaxial material to increase PL signal.

Finally, to study the effect of thermally induced dielectric stress on quantum efficiency and other device characteristics, we fabricated broad area high power laser diodes of (4 mm) $\times$ (100 μm) size with as-grown and RTA processed structures. For RTA processed laser devices, QWI with 250 nm SiO_2 and suppression capping with 2-layer (10 nm-Si_xO_2/10 nm-SrF_2) and 1-layer (10 nm-SrF_2) dielectrics were applied on neighboring emitters on the same bar. SiO_2 film was also covered by Si_xO_2/SrF_2 films to simplify the processing steps since it does not influence the QWI behavior of SiO_2 as confirmed by the PL experiments. Each emitter is covered only by the corresponding dielectric and then the whole wafer was annealed at 880 °C for 4 min. All dielectric layers were removed before the fabrication process. Ridge waveguides were formed, a dielectric layer (Si_3N_4) was deposited to act as an electrical insulator and current injection windows were opened on top of the ridge waveguides. P- and n-metals were deposited and alloyed to form contacts.
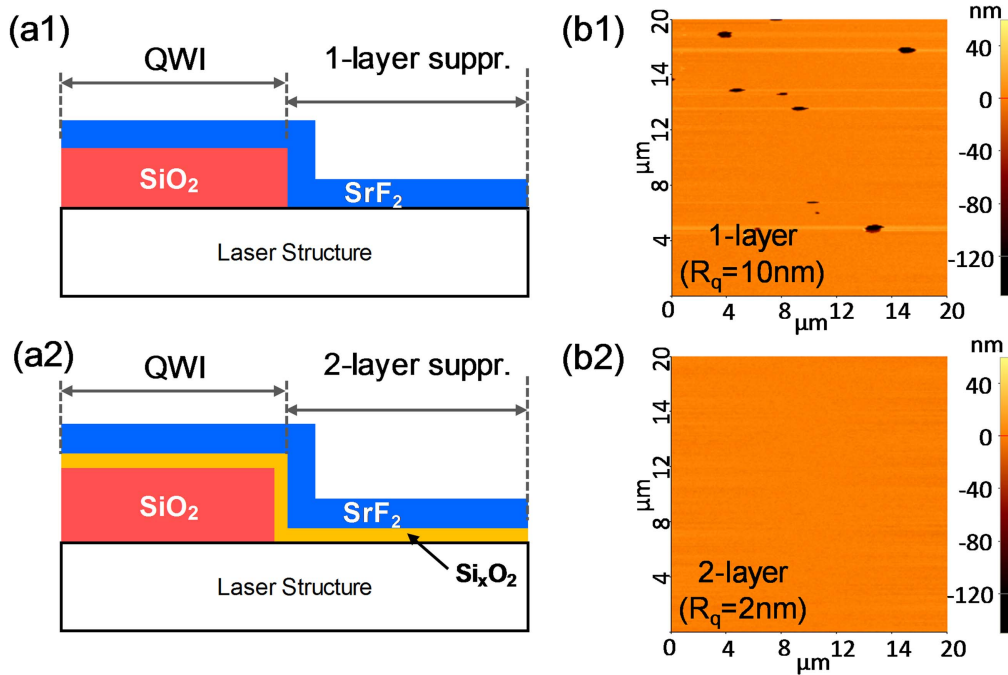
Figure 1. Side view schematic of QWI and suppression configuration investigated in this study using (a1) 1-layer and (a2) 2-layer suppression method. Corresponding top view AFM images of the (b1) 1-layer and (b2) 2-layer deposited surfaces after annealing and etching of dielectrics.

Fabricated lasers were cleaved and tested epi-side up under continuous wave current injection at room temperature.

3. Results and discussion

3.1. Intermixing with single layer versus bilayer dielectrics

Figures 1(a1) and (a2) illustrate the side view schematic of the QWI (SiO_2) and suppression regions (1-layer versus 2-layer) on top of the laser epitaxial structure. Due to different thermal stress generated by SrF_2 (1-layer) and Si_xO_2 films, a strain-compensated 2-layer (Si_xO_2/SrF_2) approach was investigated to understand the influence of thermally induced dielectric stress. The deposition recipe for Si_xO_2 was developed to yield smaller wavelength shifts, as indicated previously, in conjunction with SrF_2 for QWI suppression and with the purpose of thermal stress reduction. In these configurations, 1-layer or 2-layer suppression films also cover SiO_2 that is used for QWI; however, these films do not reduce the QWI amount of the sufficiently thick (250 nm) SiO_2 film, which was confirmed by PL measurements. Figures 1(b1) and (b2) illustrates the top view AFM images of the suppression region surfaces with 1-layer and 2-layer films after RTA for 2 min at 880 °C and etching of the dielectrics, where the color bar indicated the depth/height of the surface. Annealing induces structural changes in the SrF_2 film and surface damage after its removal was clearly observed consistent with the former observations [7, 21–23] and appeared even for 5 nm thick SrF_2 layer after RTA. The surface damage suggests the stress build-up during thermal annealing of SrF_2 and, thus, the occurrence of complete stress relaxation of the induced thermal stress

accompanied by the generation of crystal defects. In contrast, good surface morphology comparable to as-grown wafer was observed in 2-layer region as illustrated in figure 1(b2). Si_xO_2 layer as thin as 10 nm used in this study was found to be sufficient to compensate SrF_2 induced damage. The root-mean-square roughness (R_q) of the 1-layer protected surface was 10 nm, whereas 2-layer protected region was improved down to 2 nm.

For semiconductor devices, it is important to identify the structural parameters such as internal strain and thermal stress that eventually control the dislocation density and device performance. It is well known that the internal strain due to lattice mismatch of quantum well structures beyond a critical thickness and mismatch ratio would create misfit dislocations and degrade the device performance [25]. Strain-compensated growth approach provides an efficient way to balance the strain and successful growth of large lattice mismatched quantum well structures [26]. Thermal stress is an intrinsic problem for heat sinks with large thermal expansion coefficient (CTE) mismatch compared to a semiconductor laser deteriorating the reliability and lifetime of devices [27]. The influence of stress on the bandgap of QWs is well known [28] and the impact of dielectric stress on the PL wavelength shift of QWI has been demonstrated [29–31]. During QWI process, the high temperature change modifies the mechanical stress of the semiconductor/dielectric system and this is mainly caused by the CTE mismatch between the semiconductor and dielectric materials. For QWI suppression, SrF_2 has so far been one of the best dielectrics for high intermixing selectivity; however, it introduces epitaxial damage and penalty on operational parameters such as voltage, threshold, quantum efficiency making it a non-ideal

Table 1. Physical parameters of dielectric films and calculated thermal stress values of single layer films on a GaAs substrate.

Material	α (ppm $^\circ C^{-1}$)	$E_f/(1-\nu_f)$ (Gpa)	σ_{in} (GPa)	$\Delta\alpha \cdot \Delta T$	σ_{th} (GPa)	σ_{total} (GPa)
Si_xO_2	1	120	-0.2	-0.5%	$+0.6$	$+0.4$
SrF_2	28	110	0	$+1.8\%$	-2.1	-2.1
GaAs	7	—	—	—	—	—

candidate. The mismatch is extensive between SrF_2 (CTE ~ 18 ppm $^\circ C^{-1}$ at $20\,^\circ C$ and ~ 31 ppm $^\circ C^{-1}$ at IFVD temperature of around $900\,^\circ C$ corresponding to effective linear CTE ~ 28 ppm $^\circ C^{-1}$) [32] and GaAs (CTE ~ 7 ppm $^\circ C^{-1}$) [33]. Employing a low CTE dielectric of Si_xO_2 (CTE ~ 1 ppm $^\circ C^{-1}$) [34] in a bilayer configuration of Si_xO_2/SrF_2 can compensate the CTE mismatch and hence reduce thermal stress on the epitaxial structure and its associated issues. Thermal stress σ_{th} generated in a thin film on a thick substrate during a thermal treatment with temperature difference ΔT is given by $\sigma_{th} = [E_f/(1-\nu_f)]\Delta\alpha\Delta T$, where E_f is the Young modulus, ν_f is the Poisson coefficient of the thin film, and $\Delta\alpha$ is the linear thermal expansion coefficient difference between the film and substrate [29]. Table 1 summarizes the physical parameters of the dielectric and GaAs substrate materials that were used in this study. The calculated values are the thermal expansion mismatch ($\Delta\alpha \cdot \Delta T$), thermal stress ($\sigma_{th}$) and total stress ($\sigma_{total}$) generated during the annealing with $\Delta T \sim +850\,^\circ C$, which are summarized in table 1. σ_{in} is intrinsic stress contribution of the dielectrics. At room temperature, the Si_xO_2 film is under compressive stress (-0.2 GPa) but it becomes tensile ($+0.4$ GPa) with thermal expansion mismatch of -0.5%. For SrF_2, the film does not have an intrinsic stress but very high compressive stress (-2.1 GPa) with large thermal expansion mismatch of $+1.8\%$ is expected at the annealing temperature. The situation is different for 2-layer films, where reduced total stress (~ -1.7 GPa) is anticipated due to strain compensation and Si_xO_2 can also work as a barrier against SrF_2 thermal stress. Although we do not have the capability to directly measure these stress states at the annealing temperature, our simple calculations provide rough estimates of the stress values. The thermal stress of bilayer dielectrics can be further reduced by engineering the initial stress levels of each film. Deposition of higher compressive stress SiO_2 ($\sigma_{in} < -0.2$ GPa) would decrease the high temperature strain of SiO_2 film. Another approach is to deposit SrF_2 films at high temperatures (i.e. $500\,^\circ C$) that would provide tensile stressed SrF_2 films at room temperature ($\sigma_{in} \sim +1.0$ GPa) and reduce its total stress to $\sigma_{total,SrF} \sim -1.1$ GPa. By employing tensile stressed SrF_2 in bilayer films, total compressive stress generated during the thermal process would reduce to -0.7 GPa, which is -1.7 GPa in the current bilayer films. Such detailed stress engineering study and its effect on QWI selectivity and semiconductor laser performance will be the subject of future work. The effect of the reduced thermal stress and protection of epitaxy by employing 2-layer compared to 1-layer film is reflected in the significant difference in AFM images (figure 2(b)), where high-quality surface morphology is obtained by 2-layer films. The consequence of bilayer approach is first studied by PL characterization and then elaborated further by device performance results of high power semiconductor lasers.
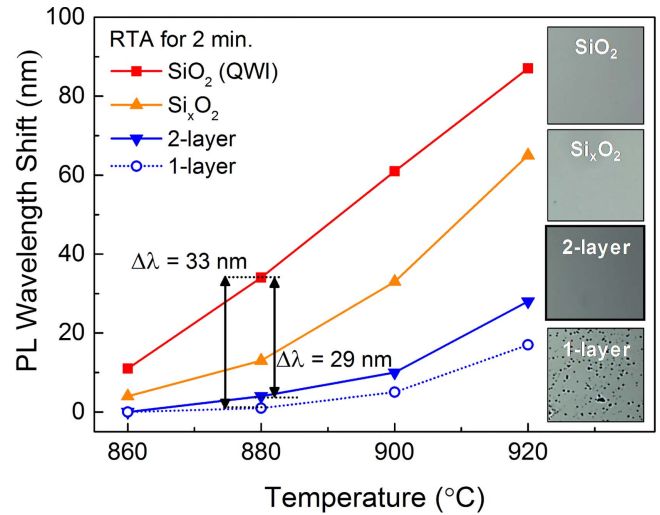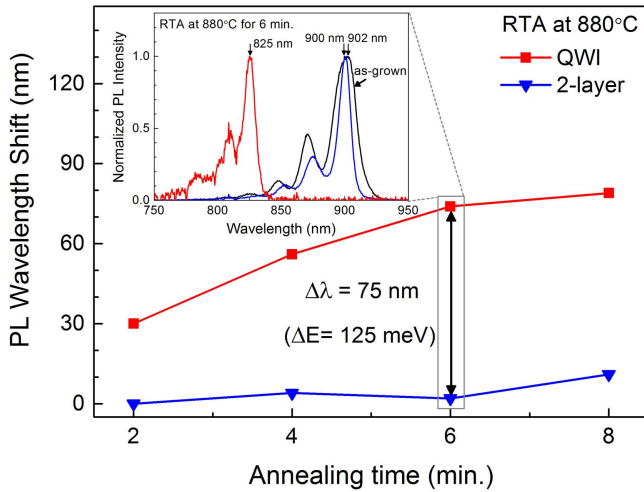

Figure 2. PL peak wavelength shift under annealing conditions of $860\,^\circ C$–$920\,^\circ C$ for 2 min. Inset shows optical micrographs of the semiconductor surface after annealing and removal of dielectrics.

Figure 2 shows the shift of the PL peak wavelength for 250 nm thick SiO_2 and Si_xO_2 versus 1-layer and 2-layer capped samples relative to the as-grown structure for annealing temperatures from $860\,^\circ C$ to $920\,^\circ C$ for 2 min. The thickness of the dielectric cap strongly affects the blue shift [35]. For both SiO_2 and Si_xO_2 layers, we found that thicknesses above 250 nm were enough to saturate QWI wavelength shift in our structure. Hence, for 250 nm SiO_2, the additional dielectric layers deposited on it did not affect its QWI behavior. 1-layer and 2-layer deposited samples clearly show that the QWI is strongly suppressed with respect to the oxide capped case. At $880\,^\circ C$, QWI selectivity was around 33 nm for a 1-layer film, whereas it decreases slightly to 29 nm for a 2-layer film. There is no substantial change in FWHM of the PL samples (not shown) indicating that the QW thickness homogeneity is preserved for both QWI and suppression regions.

3.2. Optimization of the intermixing selectivity

Figure 3 displays the effect of extended time RTA at $880\,^\circ C$ on PL wavelength shifts. It shows that the amount of QWI selectivity increases with annealing time because of the shift in QWI wavelength and the wavelength stays almost constant in the suppression region up to 6 min annealing. Longer annealing introduces more vacancies provided by the SiO_2 layer to enhance intermixing. However, the duration and temperature of RTA are not sufficient to cause disordering in the 2-layer region so that its PL wavelength is preserved. Intermixing selectivity of 75 nm (125 meV) was achieved for
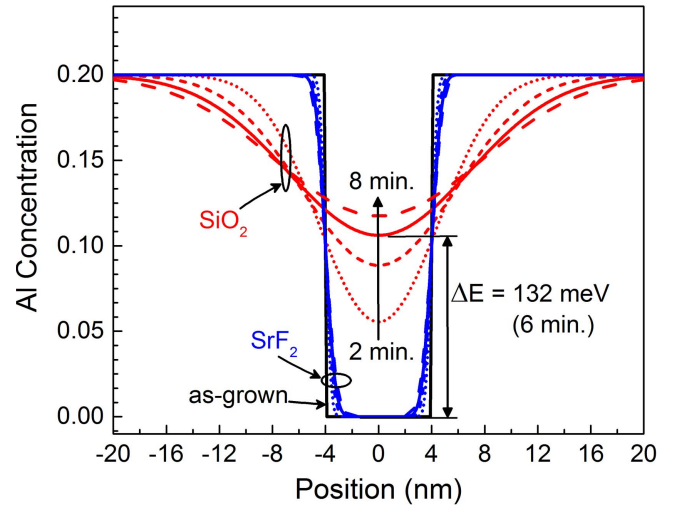
Figure 3. PL peak wavelength shift under annealing conditions of 2–8 min at 880 °C. Inset shows the PL spectrum of QWI and 2-layer suppression regions after annealing at 880 °C for 6 min compared to as-grown structure.

Figure 4. Simulation results of the change in aluminum concentration profile around the InGaAs QW in SiO$_2$ and SrF$_2$ regions for 2, 4, 6 and 8 min annealing at 880 °C compared to the as-grown profile.

6 min annealing above which the QWI region show small wavelength shift improvement with the additional time whereas the suppression region PL wavelength starts shifting. This suggests that modification of the QW potential distribution saturates most likely because a finite number of point defects in the QW material composition largely reaches equilibrium. The inset figure shows the PL spectra of QWI and 2-layer capped regions for 6 min annealing. The 2-layer region spectrum blue shifts slightly but its linewidth and QW state separations are clearly reduced. The smaller quantum state separation may be attributed to QW profile modification (e.g. Gaussian-like instead of square-like) after RTA process [36] producing smaller separations. In QWI region, the inset shows that the PL spectrum starts to smear with indistinct quantum states of the QW.

The effect of diffusion process on the compositional profiles of the barrier and QW after annealing has been reported experimentally [36] and can be examined theoretically by one-dimensional interdiffusion model following the Fick's law [15, 37]. The concentration Al(x) variation along the QW direction x can be expressed by the diffusion equation given by

$$Al(x) = Al_{bar}\left[1 + \frac{1}{2}erf\left(\frac{x - d_{QW}/2}{2L_D}\right)\right.$$
$$\left. - \frac{1}{2}erf\left(\frac{x + d_{QW}/2}{2L_D}\right)\right], \quad (1)$$

where Al$_{bar}$ is the initial Al composition in the barrier, erf(x) is the Gauss error function and d_{QW} is the QW thickness. The diffusion length is defined as $L_D = \sqrt{Dt}$, where D is the diffusion coefficient and t is the annealing time. The diffusion coefficient is a function of temperature, T, and given by $D(T) = D_0 \exp(-E_a/kT)$, where D_0 is diffusion constant, E_a is activation energy and k is the Boltzmann constant.
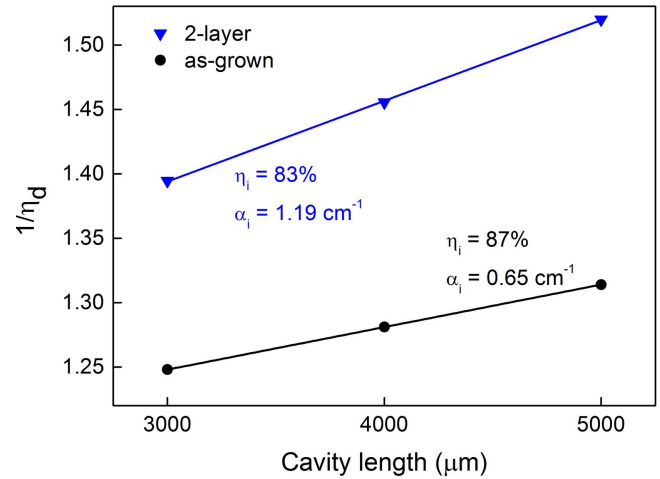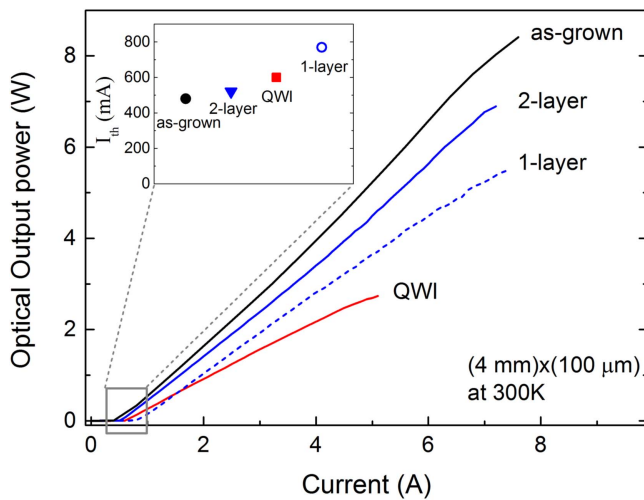
Interdiffusion occurs across the AlGaAs barrier layer and InGaAs QW. The diffusion coefficient of In with low In content of ~0.08 is assumed to be smaller compared to that of Al and Ga so that only Al–Ga interdiffusion is taken into consideration in our modeling. The diffusion equation can be applied to the barrier/QW/barrier structure with $E_a = 4.09$ eV and $D_0 = 427$ cm^2 s^{-1} for the QWI region and with $E_a = 6.40$ eV and $D_0 = 4.4 \times 10^{10}$ cm^2 s^{-1} for the suppression region [15]. This leads to diffusion coefficients of $D_{QWI} = 5.66 \times 10^{-16}$ cm^2 s^{-1} and $D_{supp.} = 4.61 \times 10^{-18}$ cm^2 s^{-1} at 880 °C, where the diffusion coefficient is around two orders of magnitude smaller in the suppression region. Diffusion parameters of SrF$_2$ capping are assumed for Si$_x$O$_2$/SrF$_2$ deposited suppression region since comparable PL shifts were realized as shown in figure 2. The diffusion equation was solved to calculate Al concentration profile along the direction normal to the 8 nm thick QW by modeling diffusion of Al into and Ga out of the QW. Figure 4 shows the simulation data for Al concentration across the barrier and QW in QWI (SiO$_2$) and suppression regions (SrF$_2$) for 2, 4, 6 and 8 min annealing at 880 °C together with the as-grown profile. In the simulations, a simple model with In$_{0.08}$Ga$_{0.90}$As QW, Al$_{0.20}$Ga$_{0.80}$As QW barriers as in the laser structure and SiO$_2$, SrF$_2$ single dielectric layers as in the experiments (but as infinite thickness sources) are assumed to calculate the bandgap profiles due to the IFVD process [15]. The variation of Al concentration modifies the bandgap, $\Delta E_g(x) = 1247$Al(x) in meV [37]. With a simplified assumption, the wavelength shift approximately follows the QW band gap at the center position, and thus the Al concentration increase to $x = 0.106$ at the center of the QW in the IFVD region corresponds to a band gap shift of 132 meV. This matches agreeably well with the experimental PL shift difference of 125 meV in figure 3 for 6 min annealing at 880 °C. Consistent with the experimental results, the simulations demonstrate that the increase of the bandgap shift is
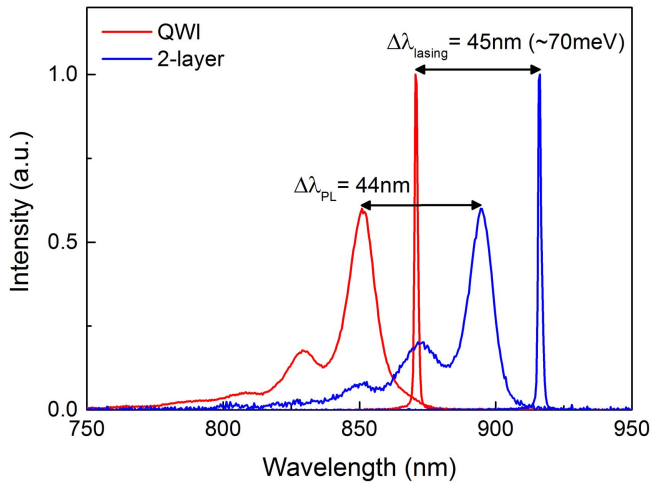
Figure 5. PL and lasing spectrum of the 2-layer and QWI regions with 4 min annealing at 880 °C.

Figure 6. Laser output power as a function of current for the as-grown structure compared to IFVD processed (4 min annealing at 880 °C) structures with 2-layer protection, 1-layer protection, and QWI lasers. The inset shows their threshold current.

Figure 7. Inverse differential efficiency versus cavity length for as grown and 2-layer protected lasers.

primarily due to QWI under SiO_2 and change of Al concentration saturates with the increase of annealing time. For the SrF_2 region, the Al concentration in the center of the QW was calculated to be unaffected but Al composition and thus the bandgap increases towards the edge of the QW. This would indicate PL peak shift to a slightly shorter wavelength and smaller QW state separations than that of the as-grown QW, which are consistent with the spectral data for 2-layer PL in figure 3 inset.

3.3. Application to high power semiconductor lasers

Based on the processes described above, broad area laser diodes were fabricated. Figure 5 shows the PL and lasing spectrum for the QWI and 2-layer capped waveguide lasers with ~45 nm (equivalent to 70 meV) difference in the emission wavelength after 4 min annealing at 880 °C. The peak wavelengths for 1-layer (not shown here) and 2-layer protected lasers are comparable to as-grown devices.

Figure 6 compares the performance of laser devices with as-grown structure and RTA processed waveguides. The lasers are tested epi side up. The slope efficiencies are 1.10, 0.99, 0.89 and 0.65 W/A corresponding to a differential quantum efficiency of 81%, 74%, 66% and 46% for as-grown, 2-layer, 1-layer and QWI lasers, respectively. The slope efficiency of the QWI laser degrades the most due to reduced confinement of the carriers as expected. Although 1-layer and 2-layer capped lasers have similar PL and lasing wavelengths, 2-layer protected device demonstrates much better slope efficiency compared to the 1-layer case. The inset of figure 6 shows the lasing threshold currents of the same devices, which are 480, 520, 600 and 770 mA for as grown, 2-layer, QWI, and 1-layer capped lasers, respectively. The threshold current of 1-layer protected laser is 60% higher than as-grown device whereas the increase is only 8% for 2-layer protected laser. Both slope efficiency and threshold performance penalty verify the degradation of epitaxial quality for the 1-layer device and better performance results using the 2-layer protection.

In order to further investigate the effect of 2-layer suppression on laser performance, internal quantum efficiency and internal loss were characterized by using reciprocal differential efficiency versus cavity length method [38]. The results are depicted in figure 7 comparing RTA processed 2-layer protected and as-grown devices. For as-grown lasers, the internal quantum efficiency and internal loss were measured as 87% and 0.65 cm^{-1}, respectively. For 2-layer capped lasers, the internal quantum efficiency and loss degraded slightly to 83% and 1.19 cm^{-1}. The internal loss increase is probably associated with the increase in the scattering losses through rough interfaces. Although 2-layer dielectric has much lower thermal stress compared to 1-layer film and it did not show any sign of epitaxial defects in AFM images, it still has large thermal stress. This stress might create rough interfaces and increase the scattering loss of the optical waveguide. For 1-layer capped lasers, we were not able to measure the internal quantum efficiency and loss parameters consistently and devices usually failed at low power levels.

However, 2-layer capped lasers exhibited similar and repeatable performance for various devices tested in this study signifying the impact of dielectric stress management of the IFVD process on laser performance.

4. Summary

In summary, we have demonstrated, for the first time, the impact of thermal stress generated by the dielectric capping layers during the IFVD process on the quantum efficiency and performance of optoelectronic devices. IFVD based QWI by SiO_2 and intermixing suppression by bilayer films of Si_xO_2/SrF_2 provided large intermixing selectivity of 75 nm (125 meV) with excellent surface morphology. Utilizing a bilayer dielectric with lower thermal stress strongly reduced the detrimental impact of the high-CTE SrF_2 film without sacrificing its QWI suppression benefits. High power laser diodes using bilayer dielectric films outperformed single-layer based approach in terms of the fundamental operational parameters of lasers. By engineering the intrinsic stress of dielectric bilayers during deposition, it is possible to reduce the thermal stress effect on IFVD process, dramatically. To achieve better performance with bilayer dielectrics, its thermal stress can further be reduced by engineering the initial stress levels of each film, i.e. by deposition of higher compressively stressed SiO_2 and tensile stressed SrF_2 dielectrics. Thermal stress engineering opens new perspectives in IFVD that would make it possible to realize large QWI selectivity together with conservation of quantum efficiency and reliable optoelectronic device performance.

Acknowledgments

ORCID iDs

Abdullah Demir ⓘ https://orcid.org/0000-0003-4678-0084

References

[1] Wenzel H, Crump P, Pietrzak A, Wang X, Erbert G and Tränkle G 2010 *New J. Phys.* **12** 085007
[2] Demir A, Peters M, Duesterberg R, Rossin V and Zucker E 2015 *IEEE Photon. Technol. Lett.* **27** 2178
[3] Demir A, Peters M, Duesterberg R, Rossin V and Zucker E 2015 *Proc. SPIE* **9348** 93480G
[4] Demir A and Peters M 2017 *US Patent* 9647416 https://www.google.com/patents/US9647416
[5] Ziegler M, Hempel M, Larsen H E, Tomm J W, Andersen P E, Clausen S, Elliott S N and Elsaesser T 2010 *Appl. Phys. Lett.* **97** 231101
[6] Epperlein P W 2013 *Semiconductor Laser Engineering, Reliability and Diagnostics: A Practical Approach to High Power and Single Mode Devices* (UK: Wiley) ch 4
[7] Ooi B S, McIlvaney K, Street M W, Helmy A S, Ayling S G, Bryce A C, Marsh J H and Roberts J S 1997 *IEEE J. Quantum Electron.* **33** 1784
[8] Furtado M T, Loural M S S, Sato E A and Sacilotti M A 1992 *Semicond. Sci. Technol.* **7** 744
[9] Du S C, Fu L, Tan H H and Jagadish C 2010 *Semicond. Sci. Technol.* **25** 055014
[10] Bryce A C, Camacho F, Cusumano P and Marsh J H 1997 *IEEE J. Sel. Top. Quantum Electron.* **3** 885
[11] Zhang X, He J J, Liu N and Dubowski J J 2015 *Opt. Express* **23** 247833
[12] Hou L, Haji M, Dylewicz R, Qiu B and Bryce A C 2011 *IEEE Photon. Technol. Lett* **23** 82
[13] Yu J S, Song J D, Lee Y T and Lim H 2002 *J. Appl. Phys.* **92** 1386
[14] Gareso P L, Buda M, Fu L, Tan H H and Jagadish C 2007 *Semicond. Sci. Technol.* **22** 988
[15] Gontijo I, Krauss T, Marsh J H and Delarue R M 1994 *IEEE J. Quantum Electron.* **30** 1189
[16] Yu J S, Song J D, Lee Y T and Lim H 2005 *Appl. Phys.* A **80** 847
[17] Kahraman A, Gür E and Aydınlı A 2016 *Semicond. Sci. Technol.* **31** 085013
[18] Pepin A, Vieu C, Schneider M, Launois H and Nissim Y 1997 *J. Vac. Sci. Technol.* B **15** 142
[19] Morita T, Nagakura T, Torii K, Takauji M, Maeda J, Miyamoto M, Miyajima H and Yoshida H 2013 *IEEE J. Selec. Top. Quantum Electron.* **19** 15002104
[20] Naito H, Nagakura T, Torii K, Takauji M, Aoshima H, Morita T, Maeda J and Yoshida H 2015 *IEEE Photon. Technol. Lett.* **27** 1660
[21] Taniguchi H, Ishii H, Minato R, Ohki Y, Namegaya T and Kasukawa A 2007 *IEEE J. Selec. Top. Quantum Electron.* **13** 1176
[22] Hofstetter D, Zappe H P, Epler J E and Riel P 1995 *Appl. Phys. Lett.* **67** 1978
[23] Hofstetter D, Maisenholder B and Zappe H P 1998 *IEEE J. Sel. Top. Quantum Electron.* **4** 794
[24] Beauvais J, Marsh J H, Kean A H, Bryce A C and Button C 1992 *Electron. Lett.* **28** 1670
[25] Chen Y C and Bhattacharya P K 1993 *J. Appl. Phys.* **73** 7789
[26] Ekins-Daukes N J, Kawaguchi K and Zhang J 2002 *Cryst. Growth Des.* **2** 287
[27] Liu X, Zhao W, Xiong L and Liu H 2015 *Packaging of High Power Semiconductor Lasers* (New York: Springer) pp 89–105
[28] Kash K *et al* 1988 *Appl. Phys. Lett.* **53** 782
[29] Pépin A, Vieu C, Schneider M, Launois H and Nissim Y 1997 *J. Vac. Sci. Technol.* B **15** 142
[30] Deenapanray P N K and Jagadish C 2001 *Electrochem. Solid-State Lett.* **4** G11
[31] Al-Jabr A A *et al* 2016 *J. Appl. Phys.* **119** 135703
[32] Roberts R B and White G K 1986 *J. Phys. C: Solid State Phys.* **19** 7167
[33] Glazov V M and Pashinkin A S 2000 *Inorg. Mater.* **36** 225
[34] Ghaderi M, de Graaf G and Wolffenbuttel R F 2016 *J. Micromech. Microeng.* **26** 084009
[35] Shimada N, Fukumoto Y, Uemukai M, Suhara T, Nishihara H and Larsson A 2001 *IEEE J. Sel. Top. Quantum Electron.* **7** 350
[36] Hulko O, Thompson D A and Simmons J G 2009 *Semicond. Sci. Technol.* **24** 045015
[37] Cibert J *et al* 1986 *Appl. Phys. Lett.* **49** 223
[38] Coldren L A, Corzine S W and Masanovic M L 2012 *Diode Lasers and Photonic Integrated Circuits* 2nd edn (New York: Wiley) p 75